Langmuir
Article
pubs.acs.org/Langmuir

Colloid Retention in Porous Media of Various Porosities: Predictions by the Hemispheres-in-Cell Model

Huilian Ma and William P. Johnson*

Department of Geology and Geophysics, University of Utah, Salt Lake City, Utah 84112

Received July 20, 2009. Revised Manuscript Received September 8, 2009

The hemispheres-in-cell model for colloid transport and deposition in simple granular filtration media preserves the utilities provided in the Happel sphere-in-cell but also incorporates features (e.g., grain-to-grain contact) that are shown to drive colloid deposition from experiments and simulations when colloid−surface repulsion exists (Ma, H.; Pedel, J.; Fife, P.; Johnson, W. P. *Environ. Sci. Technol.*, **2009**, in press). The capability of the hemispheres-in-cell model to predict colloid deposition in the absence of repulsive energy barriers for different particle sizes and fluid flow velocities was previously examined (Ma, H.; Pedel, J.; Fife, P.; Johnson, W. P. *Environ. Sci. Technol.*, **2009**, in press). In this article, we examine the influence of porosity on colloid deposition in terms of theoretical (simulated) collector efficiencies from the hemispheres-in-cell model, as well as existing models, to examine whether expected trends in porosity are similar among the different models. The need for experimentally determined collector efficiencies for porosities outside the range of 0.33−0.42 is highlighted. We demonstrate agreement between existing experimental results and our model predictions, indicating that the hemispheres-in-cell model can potentially serve as a new model geometry to develop a predictive theory of colloid filtration in the presence of energy barriers, a condition that is typical in environmental contexts.

Introduction

The transport and deposition of colloidal particles in granular porous media is important in various environmental processes, including riverbank filtration, colloid-facilitated contaminant transport, and pathogen removal in water-treatment facilities. The deposition of suspended colloids onto granular surfaces during transport is governed by the physiochemical (and/or biological) interactions of particles, suspending fluid, and porous media. The process is well understood and relatively predictable for the case when no repulsion exists between colloids and medium surfaces (conditions favorable to deposition). However, for the case when colloid−surface repulsion exists, a condition that is typical in environmental contexts, predicting colloidal retention in porous media remains a major challenge because no mechanistic, easily accessed models yet exist.

The mechanistic prediction of colloid transport and deposition in saturated porous media under favorable conditions (in the absence of repulsive energy barriers) is made possible by idealizing the porous media as being composed of unit bed elements (UBE) wherein the probability of colloid retention in a UBE is determined through particle trajectory (or flux) simulations. The trajectory (or flux) simulations are based on a mechanistic force and torque balance on the colloid within the flow field of the UBE. Among the various types of UBEs, the Happel sphere-in-cell has been widely used.[2−4] The Happel sphere-in-cell consists of a solid sphere encircled by a spherical fluid shell, where the thickness of the fluid shell is chosen such that the porosity of this unit cell (solid sphere and fluid shell) is equal to the actual porosity of a packed bed.[5] The collector efficiency (η), which is the number of colloids that attach to the collector relative to the number of colloids that enter the unit cell, is determined from mechanistic simulations within the Happel sphere-in-cell. To make the power of these mechanistic simulations accessible to nonmodelers, the simulations have been regressed to dimensionless parameters to provide phenomenological equations for the estimation of η.[2,3] These equations serve as excellent predictive tools for colloid deposition in simple porous media when energy barriers to deposition are absent.

When energy barriers to deposition are present (unfavorable conditions), the mechanistic models operating in the context of the Happel sphere-in-cell predict zero retention (i.e., no colloids overcome the repulsive energy barrier); whereas common experience demonstrates that some retention occurs despite colloid−surface repulsion. To develop mechanistic predictors of retention under unfavorable conditions, the essential mechanisms of colloid retention must be identified and incorporated. Experiments indicate that colloid retention under unfavorable conditions occurs in the following locations: (i) "holes" in the energy barrier where the energy barrier is locally reduced or eliminated by surface roughness or heterogeneity (e.g., heterodomains of attractive charge);[6,7] (ii) grain-to-grain contacts where colloids may be wedged between energy barriers and push through one of them into contact with the surface;[8,9] and (iii) zones of low fluid drag where secondary energy minimum-associated colloids may be retained without contact.[9−12]

*Corresponding author. E-mail: william.johnson@utah.edu. Tel: (801)585-5033. Fax: (801)581-7065.

(1) Ma, H.; Pedel, J.; Fife, P.; Johnson, W. P. *Environ. Sci. Technol.*, **2009**, in press.
(2) Rajagopalan, R.; Tien, C. *AIChE J.* **1976**, *22*, 523–533.
(3) Tufenkji, N.; Elimelech, M. *Environ. Sci. Technol.* **2004**, *38*, 529–536.
(4) Nelson, K. E.; Ginn, T. R. *Langmuir* **2005**, *21*, 2173–2184.
(5) Happel, J. *AIChE J.* **1958**, *4*, 197–201.
(6) Song, L.; Johnson, P. R.; Elimelech, M. *Environ. Sci. Technol.* **1994**, *28*, 1164–1171.
(7) Bhattacharjee, S.; Chun-Han, K.; Elimelech, M. *Langmuir* **1998**, *14*, 3365–3375.
(8) Li, X.; Lin, C.-L.; Miller, J. D.; Johnson, W. P. *Environ. Sci. Technol.* **2006**, *40*, 3769–3774.
(9) Johnson, W. P.; Li, X.; Yal, G. *Environ. Sci. Technol.* **2007**, *41*, 1279–1287.
(10) Hahn, M. W.; O'Melia, C. R. *Environ. Sci. Technol.* **2004**, *38*, 210–220.
(11) Kuznar, Z. A.; Elimelech, M. *Colloids Surf., A* **2007**, *294*, 156–162.
(12) Shen, C.; Li, B.; Huang, Y.; Jin, Y. *Environ. Sci. Technol.* **2007**, *41*, 6976–6982.

Colloid retention in the presence of energy barriers by these mechanisms has been demonstrated in mechanistic simulations in unit cells containing multiple grains in various packing arrangements that incorporate grain-to-grain contacts (e.g., the dense cubic packing unit).[9,13] However, these packing arrangements are not suitable to serve as predictive frameworks because of their fixed porosities and also because they do not provide a good prediction of colloid deposition in porous media in the absence of energy barriers.[9,13]

The foundation for a general colloid filtration theory (for predictions in both the absence and presence of energy barriers) needs to meet at minimum the following three criteria: (1) represent a range of porosities; (2) provide an accurate prediction of η in the absence of an energy barrier; and (3) incorporate attributes to allow colloid retention in the presence of an energy barrier (e.g., grain-to-grain contacts). In a previous paper, we proposed a new unit cell geometry, namely, the hemispheres-in-cell model, for the purpose of developing predictive capability of colloidal deposition in the presence of energy barriers.[1] The hemispheres-in-cell (Figure 1) preserves the utilities provided in the Happel sphere-in-cell (e.g., capable of representing a spectrum of porosities, with the outer fluid boundary shell serving as a "watershed divide" between adjacent collectors in the flow field) but also incorporates geometries (e.g., grain-to-grain contact) that potentially allow colloid retention in the presence of an energy barrier. Hence, the hemispheres-in-cell model is expected to behave similarly to Happel sphere-based models[2−4] in predicting colloid deposition in porous media in the absence of energy barriers.[2,3] This agreement as a function of colloid size and fluid velocity was demonstrated by Ma et al. at a fixed porosity of 0.37.[1]

In this article, we will address the issue of whether the hemispheres-in-cell model is capable of predicting colloid retention across a range of porosities. Changes in porosity alter the fluid-flow field surrounding the collectors via the influence of neighboring collectors. Thus, the transport and deposition behavior of colloids through the porous media is expected to change with porosity. The porosities that have been examined by previous filtration theory researchers generally fall within the range of 0.36−0.42.[2−4] Rajagopalan and Tien[2] developed their correlation equation for collector efficiency for a fixed porosity of 0.39 whereas Tufenkji and Elimelech[3] indicated that they had investigated a range of porosities (e.g., 0.30−0.50) but presented simulation results only for the porosity range of 0.36−0.40. More recently, Long and Hilpert[14] presented a correlation equation for the estimation of η based on an assemblage of randomly packed spheres with a porosity range of 0.30−0.42. To capture the influence of porosity on the flow field and transport in their correlation equation, they proposed to use a Carman−Kozeny-derived porosity parameter,[14] which is generally used to describe the pressure drop across a packed bed in response to porosity changes.[15] The corresponding porosity-dependent parameter employed in the Happel sphere-based model is A_s (see the Nomenclature section for its definition), which is part of the parameters that describe the flow field in the Happel sphere-in-cell.[2,5,15] The influence of these two parameters on colloid retention at different porosities will be examined.

Although these existing correlation equations all include porosity-dependent parameters, none of them have been tested against experiments or expectations from theory (e.g., trajectory models) outside the porosity range of 0.33 to 0.42, corresponding to clean porous media (spheroid and narrow size distribution) typical of the experiments supporting filtration theory. In this article, we examine the influence of porosity on theoretical (simulated) collector efficiencies from the hemispheres-in-cell model, the Happel-based models,[2−4] and the model from Long and Hilpert[14] to examine whether expected trends in porosity are similar among the different models. Disagreement among the models may spur experimental investigations of porous media to determine trends empirically outside the limited porosity range. In our simulations, three representative porosities are examined: 0.25, 0.37, and 0.48. In addition, we test the predictive capability of the hemispheres-in-cell model via comparison with existing experimental data. We emphasize here, however, that our goal is not to improve the prediction of retention under favorable conditions but rather to develop a foundation to predict colloid retention under unfavorable conditions (when energy barriers are present) because the hemispheres-in-cell model possesses the necessary features that allow the incorporation of the retention mechanisms of colloids in the presence of energy barriers, as described above.

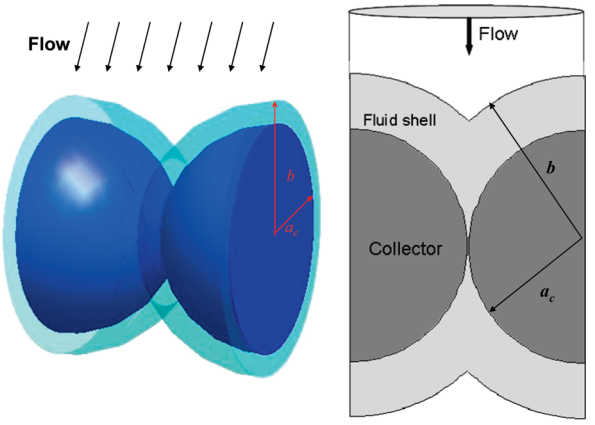

Figure 1. Three-dimensional and two-dimensional representations of the hemispheres-in-cell geometry, which contains a grain-to-grain contact and can represent a spectrum of porosities by varying the fluid shell thickness ($b - a_c$) (light sea green in 3D) relative to the collector radius (a_c) (blue in 3D). The flow is directed perpendicular to the line connecting the two-hemisphere centers.

Model Development

Hemispheres-in-Cell Model. The hemispheres-in-cell model (Figure 1) represents a spectrum of porosities in porous media by varying the outer fluid envelope radius (b) relative to the collector radius (a_c), a feature similar to the Happel sphere-in-cell. The hemispheres-in-cell incorporates a grain-to-grain contact, which does not exist in the Happel sphere, and like the Happel sphere-in-cell, the hemispheres-in-cell also contains forward and rear flow stagnation points. The porosity of the hemispheres-in-cell is related to the radii of the collector and the outer fluid envelope as follows:

$$\varepsilon = \frac{3\left(1 - \frac{a_c^2}{b^2}\right)}{3 - \frac{a_c^2}{b^2}} \text{ or } \frac{a_c}{b} = \left(\frac{3 - 3\varepsilon}{3 - \varepsilon}\right)^{1/2} \quad (1)$$

Computational Meshes and Flow-Field Simulation. To our knowledge, no closed-form solutions for the fluid-flow field in the hemispheres-in-cell yet exist; as a result, the flow field for the hemispheres-in-cell was derived using computational fluid dynamics (CFD). Computational meshes to support the numerical solution of the fluid velocities in the pore domain were first

(13) Cushing, R. S.; Lawler, D. F. *Environ. Sci. Technol.* **1998**, *32*, 3793–3801.
(14) Long, W.; Hilpert, M. *Environ. Sci. Technol.* **2009**, *43*, 4419–4424.
(15) Tien, C.; Ramarao, B. V. *Granular Filtration of Aerosols and Hydrosols*; Elsevier: Oxford, U.K., 2007.

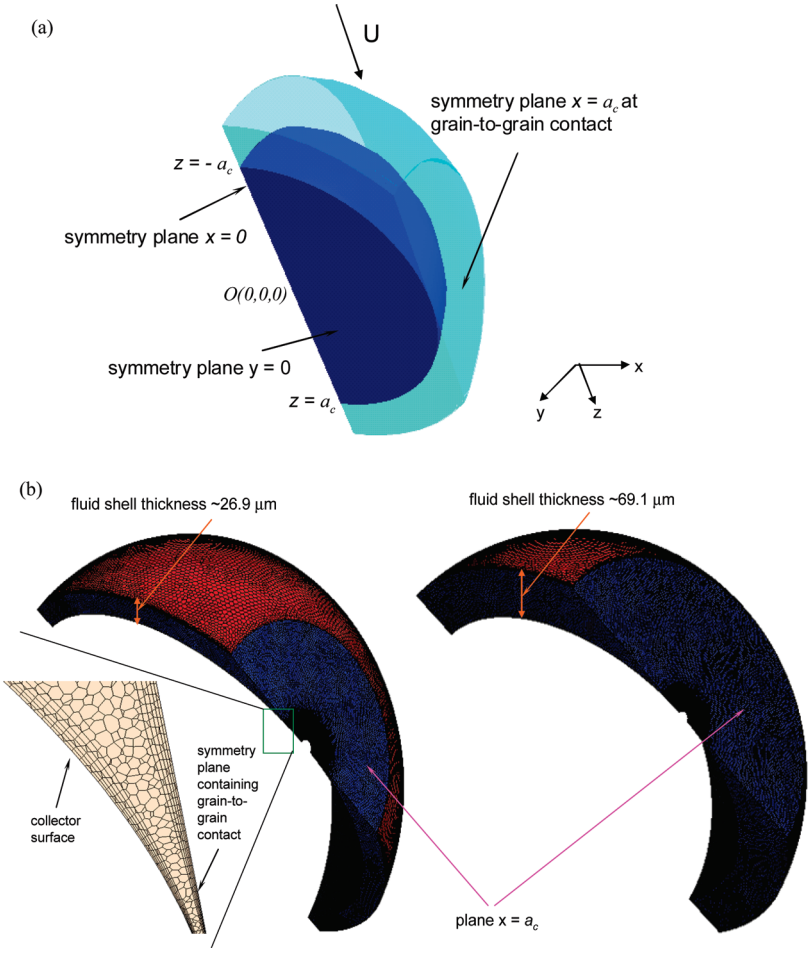

Figure 2. (a) Quadrant of the hemispheres-in-cell model confined to the quadrant defined by $x \in [0, a_c]$, $y \in [-b, 0]$ with all of the symmetry planes shown ($x = 0$, $x = a_c$, and $y = 0$). The positions of forward and rear stagnation points are indicated by $z = -a_c$ and $z = a_c$, respectively. (b) Images showing computational meshes constructed for the fluid shell in part a at different porosities (left, porosity of 0.25 with a fluid shell thickness of ~26.9 μm; right, porosity of 0.48 with a fluid shell thickness of ~69.1 μm). The inset illustrates the constructed subsurface layer mesh cells close to the collector surface and the grain-to-grain contact region.

developed using STAR-CD and Star-ccm+ software[16] (protocols for mesh construction are provided in detail in Ma et al.[1]). Because of the symmetry in the hemispheres-in-cell, it is sufficient to build the mesh for only one quadrant (e.g., the quadrant defined by $x \in [0, a_c]$, $y \in [-b, 0]$ in Figure 2a). The constructed meshes for one quadrant of the hemispheres-in-cell UBE were developed for porosities of 0.25, 0.37, and 0.48 and were composed of approximately 0.67, 1.06, and 1.29 million cells, respectively. An image demonstrating the meshes corresponding to the porosity change is shown in Figure 2b.

The flow field in the hemispheres-in-cell mesh was then derived by numerical simulation of the steady-state Navier−Stokes equation under laminar flow hydrodynamics in conjunction with the continuity equation

$$\rho_f v \cdot \nabla v = -\nabla p + \mu \nabla^2 v \qquad \nabla \cdot v = 0 \tag{2}$$

where v is the fluid velocity vector, p is the pressure, and ρ_f and μ are the density and dynamic viscosity of the fluid, respectively. Numerical simulation of the flow field was performed using the computational fluid dynamics packages STAR-CD and Star-ccm+.[16] The boundary conditions for the hemispheres-in-cell include a no-slip boundary at grain surfaces, nontangential stress and zero radial velocity at the fluid envelope outer boundary, which represents a "watershed divide" boundary between neighboring grains as in the Happel sphere-in-cell model. Symmetry boundaries were implemented at the lateral symmetry planes, and superficial fluid velocities were stipulated at the cell entry and exit planes.

The implementation of the no-tangential stress condition on the outer fluid boundary of the hemispheres-in-cell is challenging because of the presence of the grain-to-grain contact. This boundary condition is approximated via compression of the known Happel sphere nontangential stress boundary condition, as described in Ma et al.[1] The compression was carried out by a linear redistribution of boundary flow from the Happel $\pi/2$ rad arc (e.g., abc) to a shorter arc between planes $x = 0$ and $x = a_c$ (e.g., ab) along the approximated streamline arcs in the $x-z$ plane (referred to as compression A), as illustrated in Figure A1a in Appendix A. In this article, a slightly different method of compression (compression B) was used, where the boundary flow was linearly redistributed from arc abc to ab along streamline arcs emanating from the point $(0, 0, -b)$ (Figure A1b in Appendix A). The deposition behavior under favorable conditions (in the absence of an energy barrier) was found to be negligibly affected by the choice between these two different compression techniques, as shown for the 0.37 porosity (Figure 3). Subsequent simulations reported in this article were conducted using compression B.

(16) CD Adapco, computational fluid dynamics software, www.cd-adapco.com, 2007.

Particle Trajectory Analysis. Trajectories of colloids within the hemispheres-in-cell model were simulated on the basis of the classical Langevin equation

$$(m + m^*)\frac{du}{dt} = F_D + F_G + F_L + F_{EDL} + F_{vdW} + F_B \quad (3)$$

where m is the particle mass, m^* is the virtual mass (equal to one-half the displaced volume of fluid by the sphere), and u is the particle velocity vector. On the right-hand side of the above equation are forces acting on the particle, including fluid drag (F_D), gravity (F_G), shear lift (F_L), electrostatic (F_{EDL}), van der Waals (F_{vdW}), and Brownian (F_B) forces. Among the forces, F_L, F_{EDL}, and F_{vdW} act only on the particle in the normal direction relative to the collector surface. The drag forces at distances close to the collector surface were corrected as a result of hydrodynamic retardation. Expressions for these forces are briefly summarized in the Nomenclature section and in Appendix B. (For details, see Ma et al.[1] and Johnson et al.[9]) The Brownian force is modeled in our system as a Gaussian white-noise process[17−19]

$$F_B = R\sqrt{\frac{2\xi kT}{\Delta t}} \quad (4)$$

where R is a Gaussian random number with zero mean and unit variance, Δt is the time step, and ξ is the distance-dependent friction coefficient, approximated by $6\pi\mu a_p/f_1$ in the direction normal to the collector surface[20] and by $6\pi\mu a_p/f_4$ in the tangential direction,[21] where f_1 and f_4 are universal hydrodynamic functions. To approximate Brownian motion as a series of uncorrelated random movements as in eq 4, the time step employed in the trajectory simulations should be much greater than the particle momentum relaxation time (MRT),[4,22−24] which is m/ξ.

Upon resolving the particle velocity vector (Appendix B), the updated particle position is determined from $d\mathbf{x}/dt = u$, where $\mathbf{x}$ is the particle position vector. Our approach uses first-order integration with adaptive time steps that were modified to maintain changes in fluid velocity and colloidal forces below user-specified tolerances (see ref 9). The lower limit of the range of Δt values is set by the MRT as described previously. The MRT values corresponding to our simulated particle sizes in the bulk solution are given in Table 2. Δt in eq 3 should also be sufficiently small such that all forces acting on the particle can be treated as constants during a time step (trajectory step); this is especially challenging at small separation distances (<1000 nm), where colloidal interaction forces (colloid−surface and colloid−colloid forces) change drastically with separation distance. The simulated values of the collector efficiency were found to be unaffected by the time step within the range of 1 to 1000 MRT. Hence, we set the lower limit of Δt = 10 MRT. Because of the probabilistic nature of Brownian forces, a large number of particle trajectories are required to determine a robust value for the collector efficiency; here, 4000 trajectories were simulated for all porosity values (i.e., 0.25, 0.37, and 0.48) at a pore water velocity of 4 m/day.

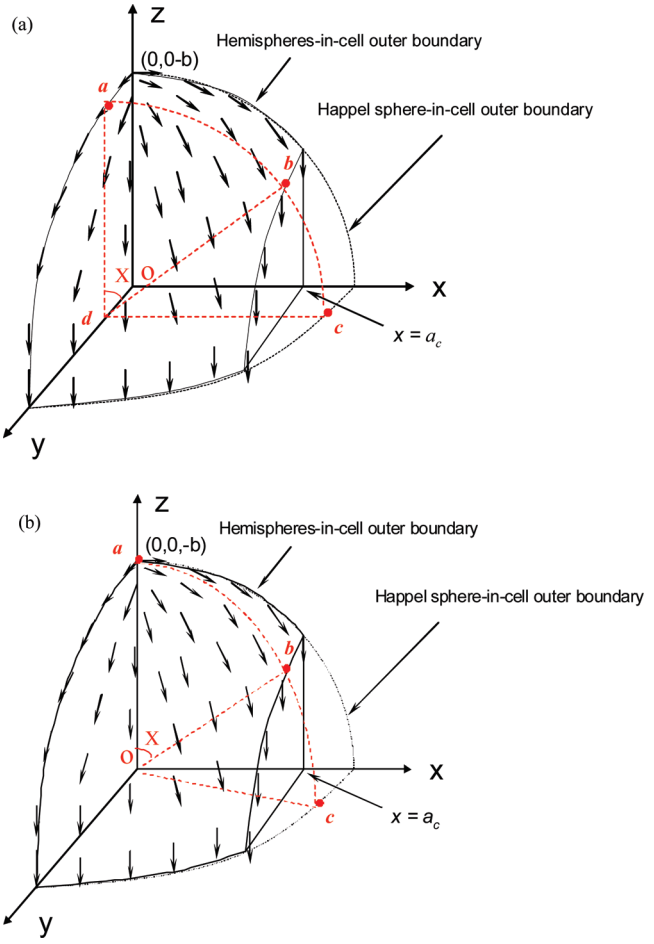

Figure A1. Sketch illustrating the implementation of the nontangential stress boundary condition of the hemispheres-in-cell model from compressing boundary flow of the Happel sphere-in-cell model. Compression is carried out by the linear redistribution of flow from the Happel $\pi/2$ radian arc (e.g., abc) to a shorter arc between planes $x = 0$ and $x = a_c$ (e.g., ab) (a) along the approximated streamline arcs in the $x-z$ plane (compression A) and (b) along the streamline arcs emanating from (0, 0, $-b$) (compression B).

Coupling Particle Trajectory Analysis to the Computational Flow Field. The entry and exit planes to the hemispheres-in-cell are located at the $z = -b$ and $z = b$ planes, respectively. At the entry plane, colloidal particles were introduced via randomly chosen x and y coordinates ranging from $x = 0$ to a_c and from $y = -b$ to 0. Particles initially located outside the fluid envelope were subject to fluid drag corresponding to the approach velocity. Once particles entered the fluid envelope, a complete force balance as described in eq 3 was executed. Particles that exit the fluid shell downstream from the grain-to-grain contact (i.e., $z > 0$) subsequently translated down gradient via fluid drag (corresponding to the approach velocity) until they exited the system at the exit plane ($z = b$).

Following the trajectory step (translation), forces acting on the particle were determined and the process was repeated until the particle exited or was retained within the collector. Evaluating the forces acting on the particle requires the determination of the fluid velocity vector at the particle location, which requires the determination of the computational mesh node closest to the particle. Because of the large number of mesh cells (~1 million), the computational expense of determining the mesh node closest to the colloid location needed to be minimized. To reduce the

(17) Kubo, R. *Rep. Prog. Phys.* **1966**, *29*, 255–284.
(18) Li, A.; Ahmadi, G. *Aerosol Sci. Technol.* **1992**, *16*, 209–226.
(19) Ounis, H.; Ahmadi, G.; McLaughlin, J. B. *J. Colloid Interface Sci.* **1991**, *143*, 266–277.
(20) Brenner, H. *Chem. Eng. Sci.* **1961**, *16*, 242–251.
(21) Adamczyk, Z.; Dabros, T.; Czarnecki, J.; van de Ven, T. G. M. *Adv. Colloid Interface Sci.* **1983**, *19*, 183–252.
(22) Chandrasekhar, S. *Rev. Mod. Phys.* **1943**, *15*, 1–89.
(23) Uhlenbeck, G. E.; Ornstein, L. S. *Phys. Rev.* **1930**, *36*, 823–841.
(24) Ermak, D. L.; McCammon, J. A. *J. Chem. Phys.* **1978**, *69*, 1352–60.

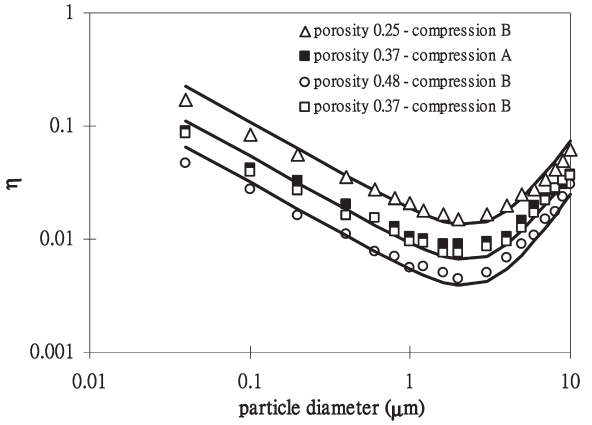

Figure 3. Simulated collector efficiencies from the hemispheres-in-cell versus particle size at three representative porosities (△, porosity 0.25; □, porosity 0.37; ○, porosity 0.48). The average pore water velocity was fixed at 4 m/day, and values for other parameters are shown in Table 1. The flow field for these simulations was obtained via compression B in Figure A1b. The solid lines are regressions from eq 6. Also shown are simulated collector efficiencies (■) at 4 m/day and porosity 0.37 using the flow field obtained via compression A in Figure A1a.

Table 1. Parameters Used in Lagrangian Trajectory Simulations

parameter	value
collector diameter, d_c	510 μm
porosity, ε	0.25−0.48
approach velocity, U	1.48 m/day
particle density, ρ_p	1055 kg/m^3
fluid density, ρ_f	998 kg/m^3
fluid viscosity, μ	9.98×10^{-4} kg·m/s
Hamaker constant, H	3.84×10^{-21} J
absolute temperature, T	298.2 K
time step, Δt	10 MRT (lower limit)

computational expense, an array was created for each velocity node that listed the neighboring velocity nodes (nodes from adjacent face-sharing mesh cells). After introducing the colloid to a particular cell at the start of the simulation, the closest velocity node was determined from the set of nodes including the original node as well as all of its neighbors, as well as the neighbors of the neighbors, to ensure the determination of the closest node in the polyhedral mesh. The distances between the colloid and the collector surfaces were computed by approximating the meshed surfaces with the ideal spherical surface. This was justified by the extremely fine discretization of the mesh at the grain surface. The lack of colloid retention on the open grain surface indicates that this approximation was reasonable.

Filter Coefficient. For the hemispheres-in-cell model, the well-known filter coefficient (λ_0) is related to the collector efficiency (η) by the following equation (its derivation is provided in detail in Ma et al.[1])

$$\lambda_0 = \frac{3(1-\varepsilon)}{2d_c}\eta\left[\frac{3-\varepsilon}{3-3\varepsilon} - \frac{2(3-\varepsilon)}{\pi(3-3\varepsilon)}\cos^{-1}\left(\frac{3-3\varepsilon}{3-\varepsilon}\right)^{1/2} + \frac{2}{\pi}\sqrt{2\left(\frac{3-\varepsilon}{3-3\varepsilon}\right)^{1/2} - 1}\right] \quad (5)$$

where d_c is the collector diameter and η is the collector efficiency, which is the number of colloids attached to the collector relative to the number of colloids that enter the unit cell (here, the hemispheres-in-cell).

Table 2. Particle Momentum Relaxation Times (MRT)

d_p (μm)	MRT (μs)	d_p (μm)	MRT (μs)	d_p (μm)	MRT (μs)
0.04	9.40×10^{-5}	1	0.059	5	1.468
0.1	5.87×10^{-4}	1.2	0.085	6	2.114
0.2	0.002	1.6	0.150	7	2.878
0.4	0.009	2	0.235	8	3.759
0.6	0.021	3	0.529	9	4.757
0.8	0.038	4	0.940	10	5.873

Results and Discussion

Effect of Porosity (and Particle Size) on Simulated Collector Efficiency. Simulated collector efficiencies from the hemisphere-in-cell model are plotted as a function of particle size at three representative porosities in Figure 3. Porosity is dictated by the thickness of the fluid shell in the hemispheres-in-cell model. However, porosity also influences the pore water velocity. The influence of the pore water velocity on η was previously examined in multiple filtration models.[1] To examine the influence on η with regard to changes in the fluid shell thickness resulting from porosity changes, we held the average pore water velocity constant and the superficial velocity was allowed to vary. The pore water velocity used for these different porosities was 4 m/day; as a result, the corresponding superficial velocities were 1, 1.48, and 1.92 m/day for simulated porosities of 0.25, 0.37, and 0.48, respectively. For a given particle size, the simulated collector efficiency decreased with increasing porosity (constant pore water velocity), as expected from the increased pore size (increased distance between collector surfaces and the fluid envelope boundary). In addition, the well-known trend in collector efficiency, showing a minimum in the 1 to 2 μm colloid size range, is observed for each porosity value in Figure 3.

Shown also in Figure 3 are predictive values of η from the correlation equation based upon the hemispheres-in-cell model as proposed in Ma et al. (shown below).[1] There is a good match between the correlation equation predictions and the numerical results for all of the porosities examined, demonstrating the predictive ability of the correlation equation

$$\eta \approx \gamma^2[2.3A_s{}^{1/3}N_R{}^{-0.080}N_{PE}{}^{-0.65}N_A{}^{0.052} + 0.55A_sN_R{}^{1.8}N_A{}^{0.15} + 0.2N_R{}^{-0.10}N_G{}^{1.1}N_A{}^{0.053}N_{PE}{}^{0.053}] \quad (6)$$

where $\gamma = (1-\varepsilon)^{1/3}$ and the dimensionless parameters (i.e., N_R, N_{PE}, N_A, N_G) and the porosity-dependent parameter A_s are defined in the Nomenclature section. The three terms in the bracket of eq 6 correspond to the contribution to η from retention mechanisms of diffusion (η_D), interception (η_I), and sedimentation (η_G), respectively. Parameter A_s was originally developed for the Happel sphere-in-cell and was adopted here because of the lack of an analytical solution to the flow field in the hemispheres-in-cell geometry, which precludes the development of the corresponding expression specific to that geometry. The good agreement of the correlation equation with the numerical simulations across a wide range of porosities (Figure 3), particles sizes (Figure 3 and Ma et al.[1]), and fluid velocities[1] indicates that A_s represents the influence of porosity on the flow-field geometry of the hemispheres-in-cell reasonably well. More discussion of A_s and another porosity-dependent parameter that was recently proposed to describe the fluid flow in a simple porous media[14] are provided in the following section.

Comparison with Existing Correlation Equations at Different Porosities. Simulated collector efficiencies from the hemispheres-in-cell model (referred to as HS) at three representative porosities at a pore water velocity of 4 m/day are compared to the

corresponding η values predicted from existing correlation equations in Figure 4. These equations include expressions for the estimation of collector efficiency from Rajagopalan and Tien[2,15,25] (hereafter referred to as the RT equation), from Tufenkji and Elimelech[3] (the TE equation), and from Long and Hilpert[14] (the LH equation). Both the RT and TE equations were developed on the basis of the Happel sphere-in-cell model, whereas the LH equation was developed from an assembly of randomly packed spherical collectors. Long and Hilpert[14] examined colloid size ranging from 0.1 to 1 μm (Brownian particles) using their packed spheres model to determine η_D. It is important to note that Long and Hilpert directly adopted η_I and η_G from the TE equation to expand their correlation equation to a larger colloid size range (> 1 μm).

Predictions differ between the LH model and the other three models (HS, TE, and RT) across all porosities, especially at higher (e.g., 0.48) and lower (0.25) porosities. At porosities of 0.37 and 0.48, the LH predictions were equal to or lower (approximately factors of 2 and 8, respectively) than the other three predictions whereas at a porosity of 0.25 the LH predictions are equal to or higher than (by a factor of ~4) η values from all of the other equations. The LH equation is distinguished from the other three models by the fact that it employs a different porosity-dependent coefficient in the diffusion term, namely, $(1 - \varepsilon)^3/\varepsilon^2$ from the Carman−Kozeny relation[14] rather than $A_s^{1/3}$ as used in the RT, TE, and HS correlation equations. These two coefficients account for the differences in η between the LH equation and the other three equations. At porosities of 0.25, 0.37, and 0.48, coefficient $(1 - \varepsilon)^3/\varepsilon^2$ has values of 6.75, 1.83, and 0.61, respectively, whereas $A_s^{1/3}$ has values of 4.86, 3.58, and 2.88, respectively. Parameter $(1 - \varepsilon)^3/\varepsilon^2$ changes by a factor of 10 in response to a change in ε from 0.25 to 0.48 whereas $A_s^{1/3}$ changes only by a factor of 2 or less over this porosity range. Note that the porosity-dependent parameter that directly comes from the Carman−Kozeny relation is actually $(1 - \varepsilon)^2/\varepsilon^3$,[15] rather than $(1 - \varepsilon)^3/\varepsilon^2$ as adapted by Long and Hilpert.[14] Nevertheless, parameter $(1 - \varepsilon)^2/\varepsilon^3$ also changes rapidly with respect to porosity (e.g., it has values of 36, 7.84, and 2.45 at porosities of 0.25, 0.37, and 0.48, respectively). Long and Hilpert[14] examined the predictability of the LH equation (including the coefficient $(1 - \varepsilon)^3/\varepsilon^2$) within a relatively small range of porosity (0.30−0.42) whereas the rapid changes in terms $(1 - \varepsilon)^3/\varepsilon^2$ and $(1 - \varepsilon)^2/\varepsilon^3$ with porosity warrants further investigation and comparison to experimental data regarding the use of this parameter. Existing data that supports filtration theory addresses a relatively narrow range of porosity (e.g., 0.33−0.42). A series of comprehensive experiments should be undertaken to explore colloid deposition in porous media having a broad range of porosities; however, these are beyond the scope of this article.

The numerical results from the HS model are in good agreement with the TE predictions across all porosities and are in good agreement with the RT predictions except at low porosity (e.g., 0.25). Specifically, our numerical results for η for colloids > 2 μm are about a factor of 2 lower than the η values predicted from the RT and TE correlation equations (except at porosity 0.48 in Figure 4c where η values from HS and RT are practically equivalent). Ma et al.[1] determined that the lesser η values predicted by the HS model resulted from the geometry change from the Happel sphere-in-cell to the hemispheres-in-cell model. The presence of the grain-to-grain contact in the HS geometry alters the flow field around the contact region and, under

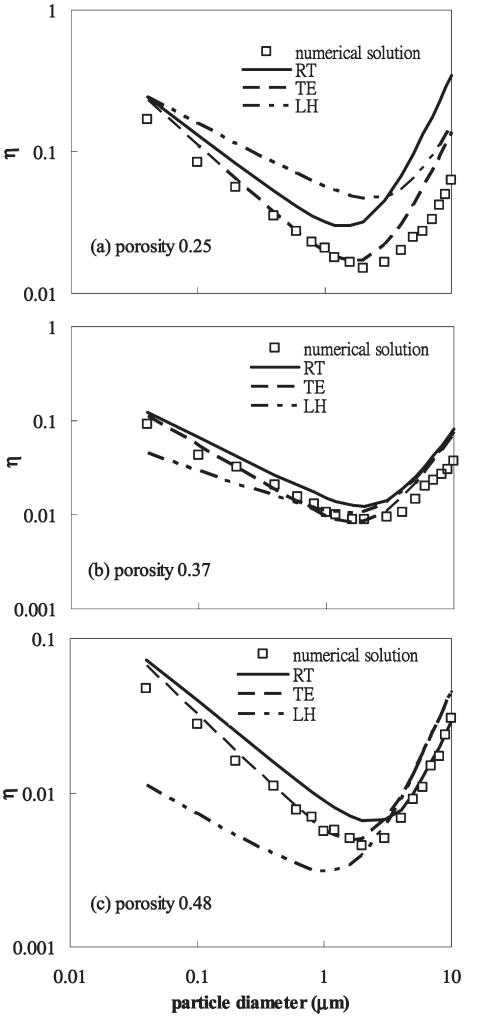

Figure 4. Comparison of simulated collector efficiencies (□) with the RT, TE, and LH predictions at different porosities at a pore water velocity of 4 m/day: (a) porosity 0.25; (b) porosity 0.37; and (c) porosity 0.48. Values for other parameters are shown in Table 1.

favorable conditions, produces slightly smaller collector efficiencies relative to the two Happel sphere-based (RT and TE) models. Note that under unfavorable conditions the grain-to-grain contact serves as a locus for wedging, which is the process of being squeezed between two energy barriers until a barrier is overcome and attachment occurs.[9] Under favorable conditions, colloids attach wherever they closely approach a surface, and wedging is not a relevant concept under this condition.

The differences in η values between the RT and TE equations for > 1-μm-sized colloids (Figure 4a,c) result from inclusion (RT) versus exclusion (TE) of parameter A_s in the sedimentation term of the correlation equation. A_s is a strong function of porosity and assumes values of about 114, 46, and 24 for porosities of 0.25, 0.37, and 0.48, respectively. The inclusion of A_s in front of the sedimentation term in the RT equation overestimates particle deposition (relative to TE) for > 1-μm-sized particles at low porosity (e.g., porosity 0.25 in Figure 4a) and slightly underestimates deposition (relative to TE) at high porosity (e.g., porosity 0.48 in Figure 4c). Within a porosity range of about $0.33 - 0.42$ (typical of well-sorted media), inclusion or exclusion of A_s in the sedimentation term is inconsequential to deposition.

For colloid sizes < 1 μm (the Brownian regime), collector efficiencies obtained from the hemispheres-in-cell are very similar to the TE predictions across all porosities examined (Figure 4),

(25) Rajagopalan, R.; Tien, C.; Tufenkji, N.; Elimelech, M. *Environ. Sci. Technol.* **2005**, *39*, 5494–5497.

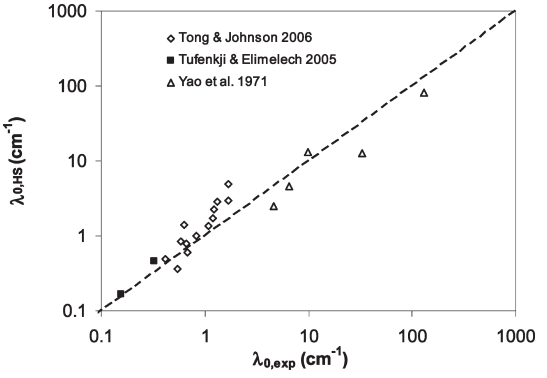

Figure 5. Comparison of experimentally measured filter coefficient (λ_0)[26−28] with those predicted from the hemispheres-in-cell model (eqs 5 and 6). These experimental data were obtained under favorable conditions, with colloid size ranging from 0.091[28] to 25.6[28] μm in diameter, pore water velocity ranging from 2[26] to 326.4[28] m/day, medium collector size ranging from 330[27] to 510[26] μm, and a porosity of 0.36[26,28] or 0.37.[27] Predictions are in good agreement with experimental data (within a factor of ~2).

except that for very small colloids (e.g., < 100 nm) HS numerical η values are slightly lower than the TE values. The reason for this difference is unclear, although it might result from the geometry change from the Happel sphere to the hemispheres-in-cell. Nelson and Ginn[4] also reported simulated η values for < 1 μm colloids in the Happel sphere system that were lower (by approximately a factor of 3) than the TE predictions for colloids.

Comparison with Experimental Data. Predictions from the hemispheres-in-cell model were compared with data from well-controlled laboratory column experiments in terms of the filter coefficient (λ_0) in Figure 5 for conditions without energy barriers. The experimental data were taken from various sources that cover a wide range of colloid size and fluid velocity and were carried out under conditions in which energy barriers to deposition are absent.[26−28] The filter coefficients for the hemispheres-in-cell were computed according to eq 5 from the corresponding collector efficiencies predicted from eq 6. The values of λ_0 predicted from the hemispheres-in-cell model match the experimentally measured values of λ_0 remarkably well (within a factor of ~2). Since all of these experiments were conducted at a porosity of ~0.36, we expect that the filter coefficients predicted on the basis of the other equations (RT, TE, and LH) also well match these measured data, where agreement among the models within this porosity range is indicated in Figure 4b. Additionally, Tufenkji and Elimelech[3] showed that the η values obtained from the TE equation fit experimentally measured η values from a variety of sources very well; hence these data are also well described by the HS model.

Our analysis indicates an opportunity to distinguish the performance of the LH and other filtration model approaches under favorable conditions via experiments at porosities outside the typical range of 0.33−0.42. Distinguishing performances among the HS, TE, and RT models under favorable conditions is not possible because they provide similar predictions for all colloid sizes, fluid velocities,[1] and porosities. These three models can be distinguished, however, by their performance in the presence of energy barriers (unfavorable conditions), under which only the HS model (among HS, RT, and TE) predicts significant colloid deposition in the presence of energy barriers greater than several kT. Subsequent papers will examine the performance of the HS model under these conditions.

Summary

Together with our previous paper,[1] we have presented the hemispheres-in-cell as a new geometry model to predict colloid transport and deposition in saturated porous media. Numerical results of the collector efficiencies from a Lagrangian trajectory analysis under a broad range of physical parameter values (e.g., particle size, fluid velocity, and porosity) under favorable conditions (energy barriers are absent) well match the predictions from the Happel sphere-based models (i.e., the RT and TE models). The LH model exhibits very different trends with respect to porosity relative to the hemispheres-in-cell, the TE, and the RT models, which warrants further experimental exploration over a broad range of porosities. Predictions from our model agree well with existing experimental data under conditions that energy barriers to deposition are absent. In a subsequent paper, we will examine the ability of the hemispheres-in-cell model to predict colloids in the presence of repulsive energy barriers, a condition that is typical in environmental contexts.

Acknowledgment. This article is based upon work supported by the National Science Foundation Chemical, Biological, and Environmental Transport and Hydrologic Science Programs (0822102) and the U.S. Department of Agriculture grant 2006-02541. Any opinions, findings, and conclusions or recommendations expressed in this material are those of the authors and do not necessarily reflect the views of the National Science Foundation or the Department of Agriculture. We are grateful for the technical and facility support provided at the Center for High Performance Computing at the University of Utah. We thank Professor Chi Tien for his valuable suggestions and input on the clarification of particle deposition processes. We also thank Professors Anthony Ladd and Jason Bulter for their useful discussions on how to represent Brownian motion in our trajectory analysis model.

Appendix A

Figure A1 illustrates the two compression techniques used to approximate the nontangential stress boundary condition on the outer fluid boundary of the hemispheres-in-cell via compression of the Happel sphere boundary flow.

Appendix B

We describe a brief summary of forces that are considered in our particle trajectory simulations. The superscript and subscript n and t refer to the normal and tangential direction to the collector surface, respectively.

The shear lift force is[29,30]

$$F_L = \frac{6.46\mu a_p^3(\partial v/\partial r)^{3/2}}{\nu^{0.5}}$$

The F_{EDL} is provided for completeness, despite the fact that we do not examine electrostatic repulsion in this article. The electrostatic double-layer force is[31]

$$F_{EDL} = 4\pi\varepsilon_r\varepsilon_0\kappa a_p\zeta_p\zeta_c\left[\frac{\exp(-\kappa h)}{1+\exp(-\kappa h)} - \frac{(\zeta_p-\zeta_c)^2}{2\zeta_p\zeta_c}\frac{\exp(-2\kappa h)}{1-\exp(-2\kappa h)}\right]$$

(26) Tong, M.; Johnson, W. P. *Environ. Sci. Technol.* **2006**, *40*, 7725–7731.
(27) Tufenkji, N.; Elimelech, M. *Langmuir* **2005**, *21*, 841–852.
(28) Yao, K.-M.; Habibian, M. T.; O'Melia, C. R. *Environ. Sci. Technol.* **1971**, *5*, 1105–1112.
(29) Saffman, P. G. *J. Fluid Mech.* **1965**, *22*, 385–400.
(30) Saffman, P. G. *J. Fluid Mech.* **1968**, *31*, 624.
(31) Hogg, R.; Healy, T. W.; Fuerstenau, D. W. *Trans. Faraday Soc.* **1966**, *62*, 1638–1651.

The van der Waals force between a spherical particle and a flat surface is[32]

$$F_{\mathrm{vdW}} = -\frac{Ha_{\mathrm{p}}}{6h^2}\frac{\lambda(\lambda+22.232h)}{(\lambda+11.116h)^2}$$

The drag force in the normal direction is[20,33]

$$F_{\mathrm{D}}{}^{\mathrm{n}} = -\frac{6\pi\mu a_{\mathrm{p}}u_{\mathrm{n}}}{f_1}+6\pi\mu a_{\mathrm{p}}v_{\mathrm{n}}f_2$$

The drag force in the tangential direction is corrected for the hydrodynamic retardation effect based on force and torque balance:[34−37]

$$F_{\mathrm{D}}^{\mathrm{t}} = -\frac{6\pi\mu a_{\mathrm{p}}u_{\mathrm{t}}}{f_4}+\frac{f_3}{f_4}6\pi\mu a_{\mathrm{p}}v_{\mathrm{t}}$$

The universal hydrodynamic functions are approximated by the following expressions:[9]

$$f_1(\bar{h}) = 1.00-0.443\exp(-1.299\bar{h})-0.5568\exp(-0.32\bar{h}^{0.75})$$

$$f_2(\bar{h}) = 1.00+1.455\exp(-1.2596\bar{h})+0.7951\exp(-0.56\bar{h}^{0.50})$$

$$f_3(\bar{h}) = 1.00-0.487\exp(-5.423\bar{h})-0.5905\exp(-37.83\bar{h}^{0.50})$$

$$f_4(\bar{h}) = 1.00-0.35\exp(-0.25\bar{h})-0.40\exp(-10.0\bar{h}^{1.00})$$

The particle velocity vector at time τ is obtained from the velocity vector at time $\tau-1$ as follows:[1]

$${u_{\mathrm{n}}}^{\tau} = \frac{\left(m+\frac{2}{3}\pi{a_{\mathrm{p}}}^3\rho_{\mathrm{f}}\right){u_{\mathrm{n}}}^{\tau-1}+(F_{\mathrm{n}}{}^{\mathrm{GRP}}+6\pi\mu a_{\mathrm{p}}v_{\mathrm{n}}f_2)\Delta t}{\left(m+\frac{2}{3}\pi{a_{\mathrm{p}}}^3\rho_{\mathrm{f}}+\frac{6\pi\mu a_{\mathrm{p}}}{f_1}\Delta t\right)}$$

$${u_t}^{\tau} = \frac{\left(m+\frac{2}{3}\pi{a_{\mathrm{p}}}^3\rho_{\mathrm{f}}\right){u_t}^{\tau-1}+\left(F_t{}^{\mathrm{GRP}}+\frac{f_3}{f_4}6\pi\mu a_{\mathrm{p}}v_t\right)\Delta t}{m+\frac{2}{3}\pi{a_{\mathrm{p}}}^3\rho_{\mathrm{f}}+\frac{1}{f_4}6\pi\mu a_{\mathrm{p}}\Delta t}$$

where $F_{\mathrm{n}}^{\mathrm{GRP}} = F_{\mathrm{G}}^{\mathrm{n}}+F_{\mathrm{L}}+F_{\mathrm{EDL}}+F_{\mathrm{vdW}}+F_{\mathrm{B}}^{\mathrm{n}}$ and $F_{\mathrm{t}}^{\mathrm{GRP}} = F_{\mathrm{G}}^{\mathrm{t}}+F_{\mathrm{B}}^{\mathrm{t}}$.

Nomenclature

a_{p}	particle radius
a_{c}	collector radius
A_{s}	neighboring grain parameter $= 2(1-\gamma^5)/(2-3\gamma+3\gamma^5-2\gamma^6)$
b	radius of fluid shell (Figure 1)
D_{BM}	diffusion coefficient $= kT/6\pi\mu a_{\mathrm{p}}$
d_{c}	collector diameter
d_{p}	particle diameter
$f_1, f_2, f_3,$ and f_4	universal hydrodynamic functions
F_{B}	Brownian force
F_{D}	drag force
F_{EDL}	electric double layer force
F_{vdW}	van der Waals forces
F_{G}	gravity $= 4\pi{a_{\mathrm{p}}}^3(\rho_{\mathrm{p}}-\rho_{\mathrm{f}})/3$
F_{L}	shear lift force
g	gravitational constant
h	surface−surface separation distance
$\bar{h}$	dimensionless separation distance $= h/a_{\mathrm{p}}$
H	Hamaker constant $= 3.84\times10^{-21}$ J
k	Boltzmann constant $= 1.381\times10^{-23}$ J/K
m	particle mass
m^*	virtual mass of particle
N_{R}	aspect ratio $= d_{\mathrm{p}}/d_{\mathrm{c}}$
N_{PE}	dimensionless Peclet number $= Ud_{\mathrm{c}}/D_{\mathrm{BM}}$
N_{A}	dimensionless attraction number $= H/(12\pi\mu{a_{\mathrm{p}}}^2U)$
N_{G}	dimensionless gravity number $= 2{a_{\mathrm{p}}}^2(\rho_{\mathrm{p}}-\rho_{\mathrm{f}})g/(9\mu U)$
R	Gaussian random number
T	absolute temperature
u	particle velocity vector
$\mathbf{x}$	particle position vector
U	approach or superficial fluid velocity
v	fluid velocity vector
v_{p}	average pore water velocity

Greek Letters

Δt	time step
ε	porosity
$\varepsilon_{\mathrm{r}}\varepsilon_0$	permittivity of water $= 7.083\times10^{-10}$ C^2/(Jm)
γ	$=(1-\varepsilon)^{1/3}$
η	collector efficiency
$\eta_{\mathrm{D}}, \eta_{\mathrm{G}},$ and η_{I}	collector efficiency due to diffusion, sedimentation, and interception, respectively
κ	Debye reciprocal length
λ	characteristic wavelength of interaction
λ_0	filter coefficient
μ	dynamic viscosity of the fluid
ν	kinematic viscosity of the fluid
ρ_{f}	density of the fluid
ρ_{p}	density of the particle
ζ_{p}	zeta potential of the particle
ζ_{c}	zeta potential of the collector
τ	time in simulation
ξ	friction coefficient

(32) Elimelech, M.; Gregory, J.; Jia, X.; Williams, R. A. *Particle Deposition and Aggregation: Measurement, Modelling, and Simulation*; Butterworth-Heinemann: Boston, 1995.
(33) Goren, S. I.; O'Neill, M. E. *Chem. Eng. Sci.* **1971**, *26*, 325–38.
(34) Goldman, A. J.; Cox, R. G.; Brenner, H. *Chem. Eng. Sci.* **1967**, *22*, 637–651.
(35) Goldman, A. J.; Cox, R. G.; Brenner, H. *Chem. Eng. Sci.* **1967**, *22*, 653–660.
(36) Spielman, L. A. *Annu. Rev. Fluid Mech.* **1977**, *9*, 297.
(37) Spielman, L. A.; Cukor, P. M. *J. Colloid Interface Sci.* **1973**, *43*, 51–65.

Langmuir
Additions and Corrections

Correction to Colloid Retention in Porous Media of Various Porosities: Predictions by the Hemispheres-in-Cell Model [*Langmuir* **2010**, *26*, 1680]. Huilian Ma and William P. Johnson*

The correct hemispheres in cell-based correlation equation for the collector efficiency (η) under favorable conditions (in the absence of repulsive energy barriers to deposition) is

$$\eta \approx \gamma^2[2.3{A_s}^{1/3}{N_R}^{-0.028}{N_{PE}}^{-0.66}{N_A}^{0.052} + 0.55A_sN_R{}^{1.8}{N_A}^{0.15} + 0.2{N_R}^{-0.047}{N_G}^{1.1}{N_{PE}}^{0.053}{N_A}^{0.053}] \quad \text{(E1)}$$

We emphasize here that the above equation (eq E1) should replace any previously published hemisphere in cell-based correlation equations (i.e., eq 3 in ref 1 or eq 6 in ref 2), shown again below (eq E2) for the estimation of η under favorable conditions.

$$\eta \approx \gamma^2[2.3{A_s}^{1/3}{N_R}^{-0.08}{N_{PE}}^{-0.65}{N_A}^{0.052} + 0.55A_sN_R{}^{1.8}{N_A}^{0.15} + 0.2{N_R}^{-0.1}{N_G}^{1.1}{N_A}^{0.053}{N_{PE}}^{0.053}] \quad \text{(E2)}$$

The differences between the correct equation (eq E1) and previously published (eq E2) correlation equations are in the exponents for parameter N_R in the first and third terms in the brackets of both equations. (Note that the slight differences in the exponents of N_{PE} in the first terms in both equations are due to decimal digit omission.)

All data presented in refs 1 and 2 reflect the correct correlation equation (i.e., eq E1).

Values of η from eq E2 are slightly larger than those from the correct equation (eq E1), typically within a factor of 1.2−1.6 depending upon the parameter conditions used (e.g., colloid size, porosity).

DOI: 10.1021/la101177d
Published on Web 04/12/2010

(1) Ma, H.; Pedel, J.; Fife, P.; Johnson, W. P. *Environ. Sci. Technol.* **2009**, *43*, 8573−8579.
(2) Ma, H.; Johnson, W. P. *Langmuir* **2010**, *26*, 1680−1687.

Correction to Experimental and Theoretical Investigation of the Catalytic Ozonation on the Surface of NiO−CuO Nanoparticles [*Langmuir* **2009**, *25*, 8001]. Wu Qin, Xin Li,* and Jingyao Qi

Pages 8001−8011. We wish to retract our article "Experimental and Theoretical Investigation of the Catalytic Ozonation on the Surface of NiO−CuO Nanoparticles", which describes that NiO−CuO nanoparticles prepared by the sol−gel method were used as a catalyst for the degradation of dichloroacetic acid by ozone.

Because of the lack of analytical equipment, our samples are usually sent to the analytical center of the school to perform analysis after experiments; we cannot conduct these experiments by ourselves. Regrettably, we made a mistake with respect to the test conditions in the gas chromatography spectrometer because of our negligence.

We apologize sincerely to the readers, referees, and editors for our mistake.

DOI: 10.1021/la100267y
Published on Web 04/27/2010

Correction to Catalytic Ozonation of Rhodamine B over CuO Catalyst Confined in Multiwalled Carbon Nanotubes: An Experimental and Theoretical Account [*Langmuir* **2009**, DOI: 10.1021/la902424z]. Wu Qin, Xin Li,* and Jingyao Qi

We wish to retract our article "Catalytic Ozonation of Rhodamine B over CuO Catalyst Confined in Multiwalled Carbon Nanotubes: An Experimental and Theoretical Account" because we do not consider the article to be suitable for the Langmuir audience.

DOI: 10.1021/la101104k
Published on Web 04/27/2010